Check for updates

Antiproliferative activity of a series of copper(II) complexes derived from a furan-containing N-acylhydrazone: monomers, dimers, charge status, and cell mechanistic studies on triple negative breast cancer cells†

Olivia Espindola-Moreno,[a] Fagner da Silva Moura,[b] Lucía Santa Maria de la Parra,[a] Carolina Stellet,[b] Jilder D. P. Serna,[c] Renata Diniz,[d] Nicolás A. Rey [ID] *[b] and Ignacio E. León [ID] *[a,e]

In this work, we evaluated the anticancer activity of compounds **1** (mononuclear) and **2** (dinuclear) copper(II) coordination compounds derived from the ligand 5-methylsalicylaldehyde 2-furoyl hydrazone (**H₂L**) over MDA-MB-231 Triple-negative breast cancer (TNBC) cells, and compared their activities with that of a newly synthesized, protonated, dinuclear analogue of **2** (complex **3**). Here, we report the synthesis of compound **3** and it has been characterized in the solid state (X-ray diffraction, FTIR) and in solution (EPR, UV-Vis, ESI) as well as its electrochemical profile. Complexes **1–3** impaired cell viability from 0.5 to 2.5 μM, with IC_{50} values around 1.25 μM for complexes **2** and **3** and a slightly higher value of 2.0 μM for the monomer **1**. It is important to highlight that the three compounds are more active than cisplatin (CDDP), by a factor of 100 in the case of **2** and **3**. Our results indicate that the protonation status of the amide group in **H₂L** plays an important role in the stability of the dimer, being compound **2** (amide-deprotonated) fairly stable in solution so we decided to continue the study of mechanism of action using this compound. Complex **2** increases the ROS production and induces cell programmed death on TNBC cells at very low micromolar concentrations (0.5–1.5 μM). Moreover, the compound decreased the amount of breast CSCs on MDA-MB-231 cells reducing the percentage of CD44+/CD24−/low cells at 1 and 1.5 μM.

[a]CEQUINOR (UNLP, CCT-CONICET La Plata, asociado a CIC), Departamento de Química, Facultad de Ciencias Exactas, Universidad Nacional de La Plata, Blvd. 120 No. 1465, La Plata (1900), Argentina. E-mail: ileon@biol.unlp.edu.ar

[b]LABSO-Bio (CTC, PUC-Rio), Departamento de Química, Pontifícia Universade Católica do Rio de Janeiro, Rua Marquês de São Vicente, 225 – Gávea, Rio de Janeiro (22453-900), RJ, Brasil. E-mail: nicoarey@puc-rio.br

[c]Centro Brasileiro de Pesquisas Físicas, Rua Dr. Xavier Sigaud, 150 – Botafogo, Rio de Janeiro (22290-180), RJ, Brasil

[d]Grupo de Cristalografia Química (ICEx, UFMG), Departamento de Química, Universidade Federal de Minas Gerais, Av. Presidente Antônio Carlos, 6627 – Pampulha, Belo Horizonte (31270-901), MG, Brasil

[e]Cátedra de Fisiopatología, Departamento de Ciencias Biológicas, Facultad de Ciencias Exactas, Universidad Nacional de La Plata, 47 y 115, La Plata 1900, Argentina

†Electronic supplementary information (ESI) available: Fig. SM1: UV-Vis stability evaluation for complexes **2** and **3** at 2×10^{-5} mol L⁻¹, under conditions similar to those in cell studies (0.5% DMSO/PBS, pH 7.4), monitored over 24 h. Fig. SM2: Apoptosis dot plots on MDA-MB-231 cells treated with complex **2** (0.5, 1 and 1.5 μM) obtained by flow cytometry. Fig. SM3: CSC dot plots on MDA-MB-231 cells treated with complex **2** (0.5, 1 and 1.5 μM) obtained by flow cytometry. CCDC 2370060 (**3**). For ESI and crystallographic data in CIF or other electronic format see DOI: https://doi.org/10.1039/d4dt03445g

Introduction

Breast cancer is one of the most common malignancies in women, with a projected 2.3 million cases by 2030.[1] One of the most aggressive types is TNBC, which accounts for around 15% of cases and is associated with a poor prognosis and the chemotherapy commonly used to treat it shows severe side effects.[2] Thus, different groups around the world focused their efforts to develop different approaches using new therapeutic agents to improve and optimize the treatment.[3]

Transition metal complexes are a new class of antitumor agents broadly used in the treatment of several solid tumors including ovarian, breast, colorectal, bone, liver, and lung.[4–6] Within the non-platinum-based compounds,[7,8] copper complexes have demonstrated promising anticancer activity tested in several experimental models,[9–15] both *in vitro* and *in vivo*. Moreover, the anti-angiogenic and anti-metastatic properties of copper(II) complexes have been reported.[16] It is important to highlight that different copper complexes are active despite

their ligands not showing a substantial cytotoxicity, evidencing the central role of the metal ion itself in the antitumor activity.[17,18] Besides, hydrazones and, more specifically, *N*-acylhydrazones and their metal complexes have attracted a remarkable interest due to their potential pharmacological activities.[19–21] In this context, our groups designed, synthetized and tested several mono- and dinuclear copper(II)-*N*-acyl-hydrazone complexes with antiproliferative activity on several solid tumor lines, including TNBC cells.[22–27]

As part of our broader study on the interaction of transition metals with hydrazones, we have recently published a mononuclear (**1**) and a dinuclear (**2**) copper(II) coordination compounds derived from the ligand 5-methylsalicylaldehyde 2-furoyl hydrazone (**H₂L**).[28] Complex **2** is a deprotonated, electrically neutral dimer of **1**. In this work, we assessed the antiproliferative profile of compounds **1** and **2** over MDA-MB-231 TNBC cells, and compared their activities with that of a newly synthesized, protonated, dinuclear analogue of **2** (complex **3**). Besides being positively charged in solution, **3** is also, in fact, a more accurate dimer of hydrolyzed (chloride ligand lost) compound **1**, in the sense that the hydrazone in both species presents the same protonation status. The expected forms in freshly prepared DMF solutions of complexes **1**, **2** and **3** are depicted in Scheme 1. However, solvolysis can quickly modify the structures of **1** and **3**, as discussed in the Results section, generating a common derivative. A complete experimental characterization of **3**, including single-crystal X-ray diffraction, was performed. FTIR, EPR, electronic absorption spectra and ESI-MS(+) were measured, as well as the electric conductivity and electrochemical profile. As for the previously reported compounds, the interactions of **3** with HSA were studied too.

Working with this structurally-related set of complexes allowed us to get a glimpse of the effect of dimerization and net charge in the anticancer activity. Moreover, we have investigated and report herein, for the first time, the mechanism of action of **2**, the most stable of the complexes considered, on MDA-MB-231 cells. Our research was focused on the role of oxidative stress and its effects on apoptosis. Furthermore, we studied the inhibition effect of the compound toward breast cancer stem cells (BCSCs).

Results and discussion

Single-crystal X-ray diffractions study

As in the case of ligand **H₂L**, and complexes **1** and **2**, the new coordination compound specifically synthesized for this work, **3**, was characterized crystallographically.

Table 1 lists the crystallographic details for **3**. The crystal structure investigation of this complex indicates that it crystallizes in the triclinic system, space group $P\bar{1}$, with two asymmetric units formed by one partially deprotonated (**HL⁻**) hydrazonic ligand, one nitrate ion, one cupric center and a water molecule (Fig. 1a) per unit cell. Asymmetric units are arranged into dimeric structures (Fig. 1b), for which Table 2

Table 1 Crystal data and refinement parameters for the dimeric copper(II) complex **3**

Formula of the monomer	$C_{26}H_{26}N_6O_{14}Cu_2$
M_r/g mol⁻¹	773.60
Crystal system, space group	Triclinic, $P\bar{1}$
Temperature/K	298
a/Å	7.1609(1)
b/Å	10.7439(2)
c/Å	11.0077(3)
α/°	61.876(3)
β/°	84.989(2)
γ/°	81.589(2)
V/Å³	1774.5(2)
Z	2
Radiation type	Cu Kα
μ/mm⁻¹	2.516
Crystal size/mm	0.03 × 0.07 × 0.19
Measured/independent reflections	30 781/3153
Observed reflections/R_{int}	2937/0.0630
Parameters	222
R_{obs}, R_{all}	0.0659, 0.0684
wR_{abs}, wR_{all}, S	0.2277, 0.2287, 1.157
$\Delta\rho_{max}$, $\Delta\rho_{min}$/e Å⁻³	1.286, −0.539
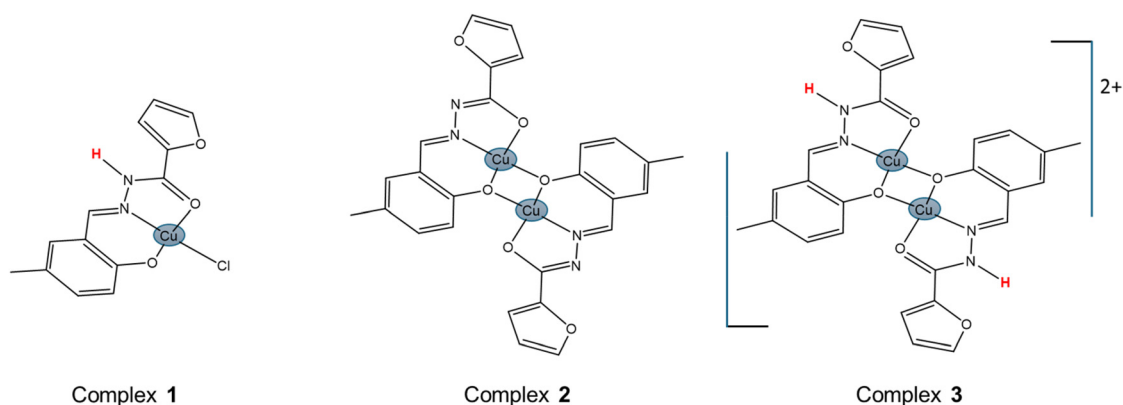
Scheme 1 Chemical structures of the mononuclear compound **1** and its deprotonated (neutral) and protonated (cationic) di-μ-phenoxo dimeric forms **2** and **3**, respectively, as characterized in fresh DMF solutions. Copper(II) centres are highlighted in blue colour and the acidic amido hydrogen of the hydrazone, in red.
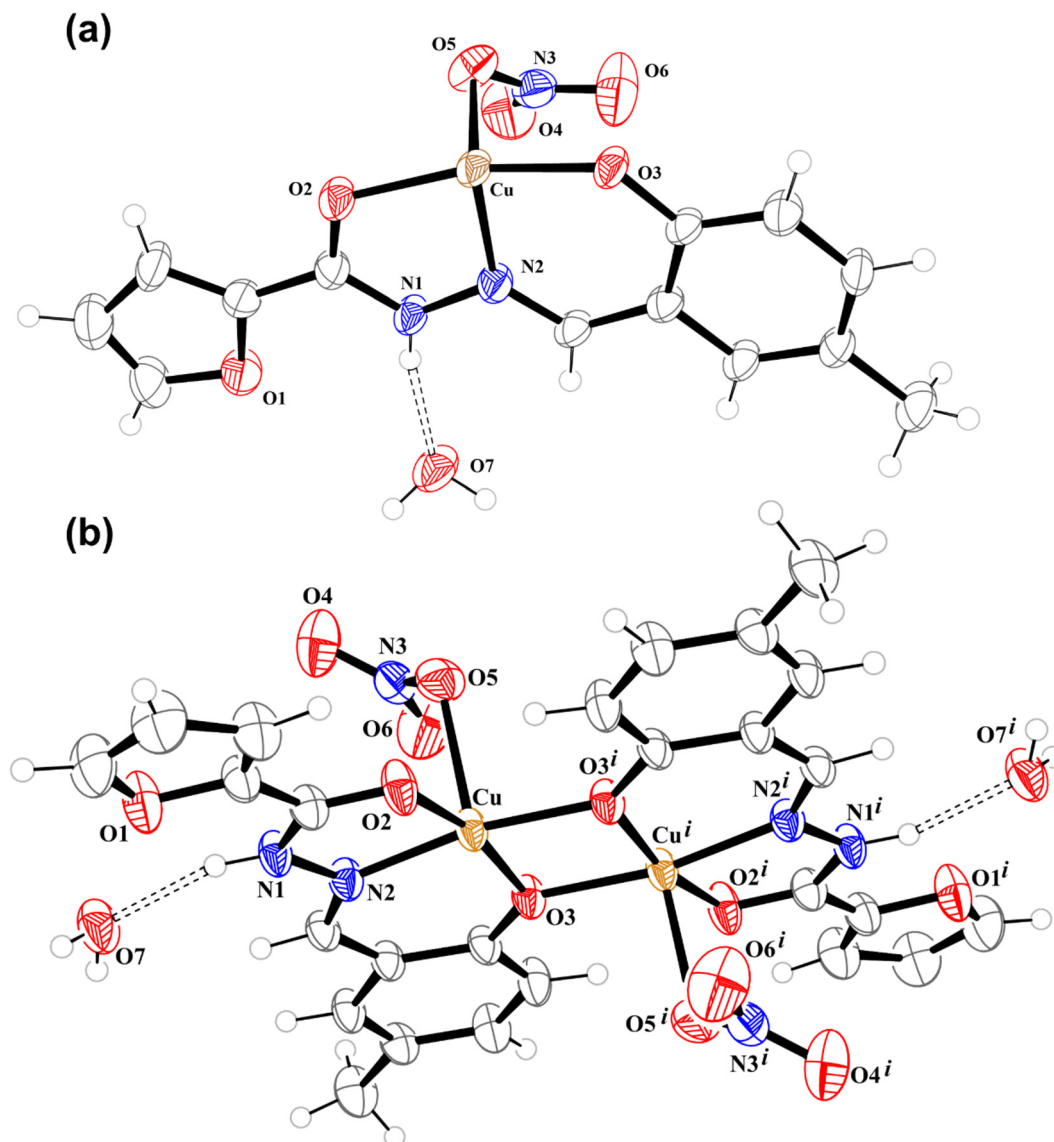
Fig. 1 Crystal structure representations of **3**: (a) asymmetric unit and (b) dimeric structure. Ellipsoids drawn at 50% probability level. Symmetry code: *i* (−*x*, 1 − *y*, 1 − *z*).

displays some selected geometrical parameters. Each metal site in the dimer is pentacoordinate in a slightly distorted square pyramidal geometry (τ equal to 0.045). Similar to the structure previously described by us for the analogue **2**, the *N*-acylhydrazone performs as a tridentate equatorial ligand through the carbonyl oxygen O2, azomethine nitrogen N2 and (ionized) phenolate oxygen O3, which acts as a bridge between both copper(II) centres. Cu···Cu distance is 2.9846(19) Å, a little bit shorter than the one reported by us for complex **2**. This coordination plane is completed by the bridging-phenolate oxygen of a second asymmetric unit (O3^i, symmetry code: −*x*, 1 − *y*, 1 − *z*), thus establishing the dimeric Cu^{2+}-(μ-phenoxo)$_2$-Cu^{2+} scaffold. Average Cu-equatorial donor distance is 1.954(5) Å. An oxygen atom (O5) from a nitrate ion occupies the fifth, apical position, in each of the metal sites, where they

point out to different sides of the dimer plane. Cu–O5 distance is 2.314(6) Å due to the Jahn–Teller effect.

As mentioned above, two crystallization water molecules per dimer are also present in the structure, which are involved in hydrogen bonding with the nitrate ion and **HL**$^−$, giving rise to a bidimensional (2D) network arrangement along the *ab* plane. The average of O···O and N···O distances (Table 2) are 2.814(10) and 2.729(9) Å, respectively.

Electronic absorption spectroscopy – a complexation study

The UV-Vis spectrum of ligand **H₂L** was already reported and fully discussed by us in a previous paper.[28] When titrating a 2 × 10^{-5} mol L^{-1} solution of **H₂L** in MeOH with successive 0.05 eq. increments of a copper(II) nitrate trihydrate methanolic solution, important spectral changes are observed (Fig. 2a). A

Table 2 Select bond distances and angles, as well as H-bonding parameters, for **3**

Bond distances/Å

Cu–O2	1.976(5)
Cu–O3	1.941(4)
Cu–O3^i	1.960(4)
Cu–N2	1.939(5)
Cu–O5	2.314(6)
Cu⋯Cu^i	2.9846(19)

Bond angles/°

O2–Cu–O3	167.0(2)
O2–Cu–O3^i	105.44(19)
O2–Cu–O5	87.0(2)
O2–Cu–N2	81.0(2)
O3–Cu–O3^i	80.20(19)
O3–Cu–O5	87.0(2)
O3–Cu–N2	91.9(2)
O5–Cu–O3^i	94.1(2)
O5–Cu–N2	94.3(2)
N2–Cu–O3^i	169.7(2)
Cu–O3–Cu^i	99.80(19)

H-bonding parameters

D–H⋯A	D–H/Å	H⋯A/Å	D⋯A/Å	D–H⋯A/°
O7–H7A⋯O5	0.85	2.01	2.843(9)	165.0
O7–H7B⋯O4	0.85	2.01	2.784(10)	150.0
N1–H1⋯O7	0.86	1.90	2.729(9)	163.0

Symmetry code: i ($-x$, $1 - y$, $1 - z$).

series of isosbestic points is clearly present at 283, 305, 327 and 367 nm, indicating the coexistence of only two absorbent species in equilibrium, *i.e.* free and copper-bound *N*-acylhydrazone. Plotting the absorbance at 412 nm as a function of the number of Cu^{2+} equivalents give rise to a classical saturation pattern, which points to a 1 : 1 stoichiometry (Fig. 2a, inset). As the reaction medium is the same used during the synthesis of complex **3**, this result provides a mechanism by which the dinuclear species can be obtained: the initial formation of [Cu(**HL**)(MeOH)]$^+$ followed by a dimerization equilibrium into the form [Cu(**HL**)]$_2^{2+}$. However, the latter step would only occur after days of slow solvent evaporation, increasing [Cu(**HL**)(MeOH)]$^+$ concentration to the point where dimerization is favored and dimer precipitation occurs. When the synthesized solid is dissolved in DMF, almost the same absorption profile is observed, although the *N*-acylhydrazone-related bands, present between 280 and 325 nm in methanolic solution, are bathochromically shifted (Fig. 2b and Table 3) due to the different nature of the solvent (*i.e.*, protic *vs.* aprotic).

In DMF solution, **3** presents a d–d absorption centred at around 688 nm, which is much closer to the one of the mononuclear complex **1** (678 nm) than to the dinuclear compound **2** (630 nm), suggesting that **3** undergoes dissociation to its monomers in solution (Fig. 2c).

Fig. 2 (a) UV-Vis titration of a 5.0×10^{-5} mol L^{-1} methanolic solution of H$_2$**L** with copper(II) nitrate trihydrate, at room temperature. Inset: absorbance at 412 nm as a function of Cu^{2+} equivalents. (b) Electronic spectrum of complex **3** (5.0×10^{-5} mol L^{-1}) in DMF. (c) The d−d absorptions' region (5.0×10^{-3} mol L^{-1}).

EPR, electrochemical and ESI-MS profiles: supporting dimer dissociation

Complex **3** is virtually EPR-silent in the solid state, due to an antiferromagnetic coupling between the copper(II) centres at close proximity [2.9846(19) Å]. Conversely, frozen DMF and
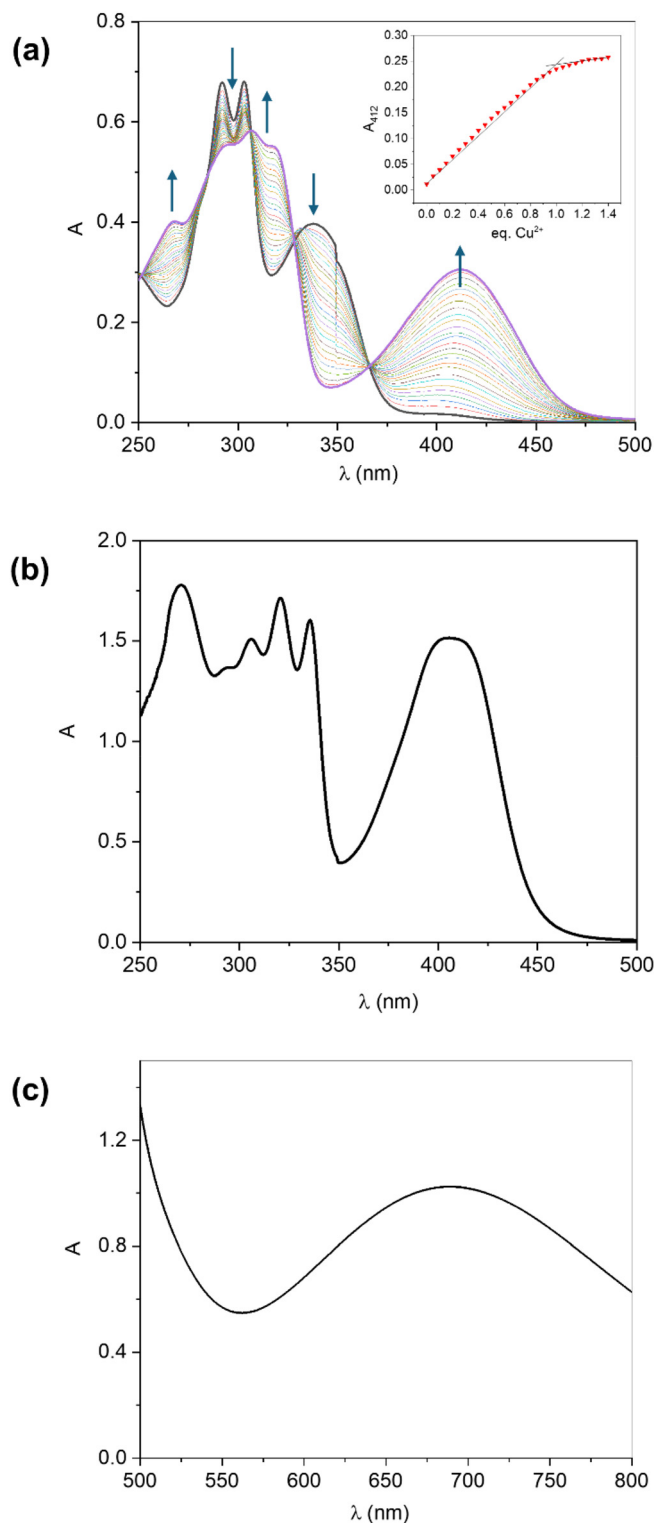
Table 3 Electronic absorption data for complex **3** in DMF solution, at room temperature

λ_{max} (nm)	ε (L mol^{-1} cm^{-1})	Assignment
270	$36\,500 \pm 2000$	Intra-ligand
305	$29\,400 \pm 405$	Intra-ligand
320	$35\,000 \pm 780$	Intra-ligand
336	$33\,900 \pm 1020$	Intra-ligand
406	$32\,150 \pm 1140$	LMCT
688	202 ± 1	d–d transition

Table 4 EPR parameters for complexes **3** in frozen (77 K) DMF and DMSO solutions

Solvent	$g_\parallel$	$g_\perp$	$A_\parallel$ (10^{-4} cm^{-1})	$A_\perp$ (10^{-4} cm^{-1})
DMF	2.26	2.05	165	11.7
DMSO	2.27	2.05	163	2.8

DMSO solutions of this complex exhibit axial spectra with well-resolved parallel and partially resolved perpendicular copper-related hyperfine splitting patterns (Fig. 3), indicating, once again, that the dimer is broken to [Cu(**HL**)DMF]$^+$ and [Cu(**HL**)DMSO]$^+$ upon dissolution in DMF and DMSO, respectively. EPR data are summarized in Table 4.

In both cases, the fact that $g_\parallel > g_\perp > 2.0023$ constitutes an indicative of unpaired electron localization in the d$_{x^2-y^2}$ orbital of copper, which points to a tetragonal symmetry around the metal centre, although heavily distorted, since Sakaguchi[29] ratios, *i.e.*, $g_\parallel/A_\parallel$, equal to 137 cm (DMF) and 139 cm (DMSO) were calculated. We also estimated the covalency parameter α2, given by the equation proposed by Kivelson and Neiman:[30]

$$\alpha^2 = \left(\frac{A}{0.036}\right) + (g_\parallel - 2.0023) + \frac{3}{7}(g_\perp - 2.0023) + 0.04$$

If the value of α^2 is 0.5, it suggests a complete covalent bonding, while a value of 1.0 means an entire ionic bonding. We obtained $\alpha^2 = 0.78$ for both solvents, which indicate that the donor-metal bonds in the complexes have an intermediate covalent character.

The same conclusion, regarding dimer dissociation, can be taken from electrochemical data measured in DMF. Fig. 4 presents the cyclic voltammogram of **3** at 100 mV s^{-1}. It is possible to observe a major cathodic peak at −0.88 V *vs.* Ag/AgCl, related to a one-electron process, altogether with a poorly defined shoulder at less negative potentials (around −0.70 V *vs.* Ag/AgCl). On the other hand, only an anodic peak (at −0.60 V *vs.* Ag/AgCl) was identified, which involves a very low current. In order to better interpreting the results obtained, we compared this electrochemical profile with the one previously published by us for the mononuclear complex **1** under the same conditions (dashed voltammogram in the figure). It became clear that the redox processes at −0.88 V and −0.60 V *vs.* Ag/AgCl are related to the presence of the solvolyzed form of **1**, [Cu(**HL**)(DMF)]$^+$, indicating that most of the dimeric nature of compound **3** is lost through dissociation in solution. The unresolved reduction shoulder observed at around −0.70 V *vs.* Ag/AgCl is probably associated with a remnant of the cationic dimer in DMF, although this could not be completely established.

ESI-MS(+) studies performed after dissolution of **3** in DMSO (as in the cytotoxicity studies discussed below) and subsequent 200x dilution in MeOH (Fig. 5), show that only one major species can be distinguished in the range between 300 and 800 Da, at (*m/z*) 384.02, corresponding to the mononuclear, cationic compound [Cu(**HL**)(DMSO)]$^+$. This was clearly confirmed based on the isotopic distribution analysis presented in the inset of Fig. 5. The detection of this DMSO-containing complex indicates a strong affinity of the copper centre by dimethyl sulfoxide, even in a methanol rich medium.

HSA-binding assessment

Fig. 6 shows the spectral changes in the 300–500 nm region produced by the addition of successive amounts of HSA to a 2 × 10^{-5} mol L^{-1} solution of complex **3**. We observe a clear bathochromic effect in all the bands of the spectrum as the titration progresses. Isosbestic points could be clearly identified at 330, 345 and 404 nm, indicating the presence of only two
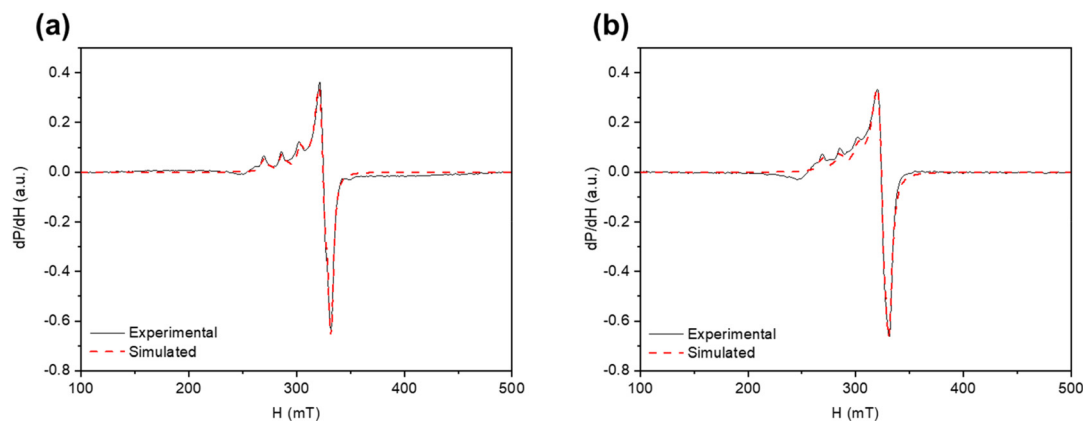
Fig. 3 X-band EPR spectra of complex **3** in frozen (77 K) solution of (a) DMF and (b) DMSO. Simulated profiles are given as dashed red lines.
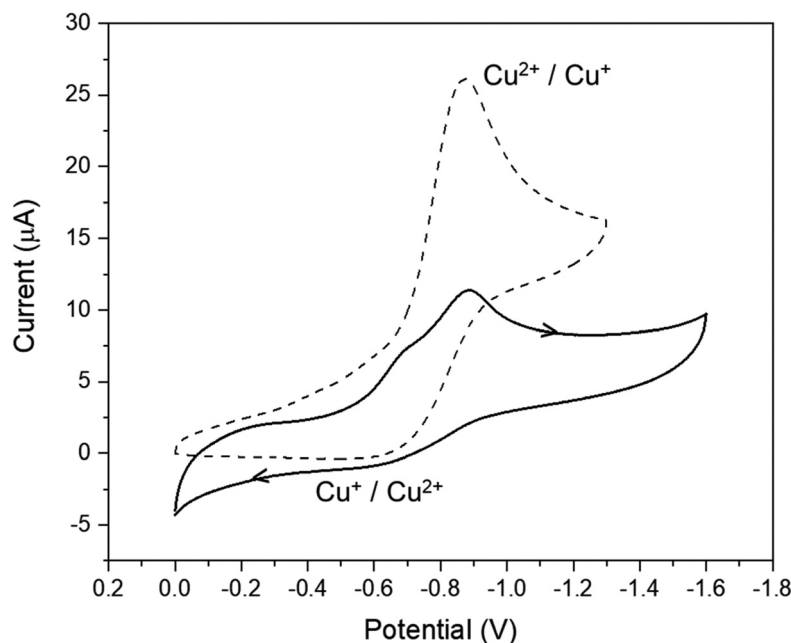
Fig. 4 Cyclic voltammogram of **3**, at the scan rate of 100 mV s^{-1}, measured in DMF/0.1 mol L^{-1} Bu$_4$NPF$_6$ (25 °C), using a Glassy Carbon Electrode as the working electrode. The cyclic voltammogram of complex **1** under the same conditions was included for the sake of comparison (black dashed curve).
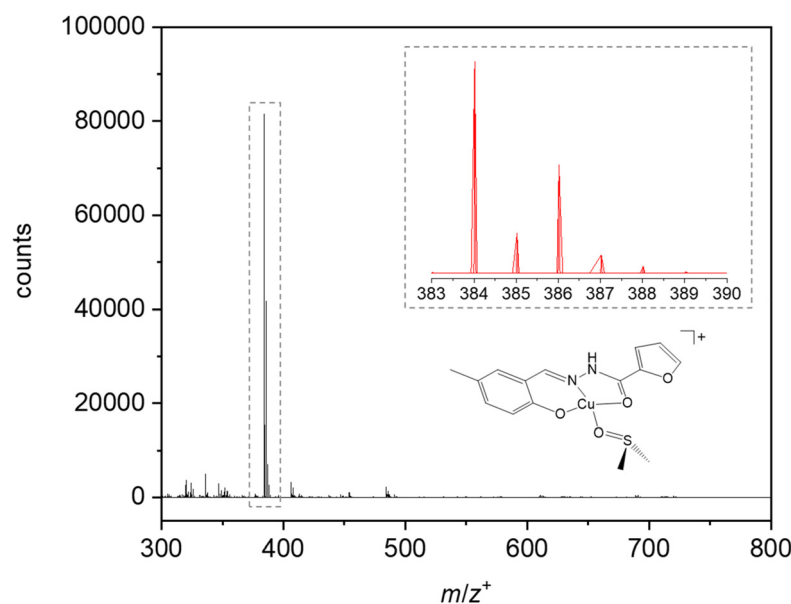

Fig. 5 ESI-MS spectrum (positive mode) of **3** in a DMSO/methanol (0.5 : 99.5) mixture. Inset: isotope distribution pattern for [Cu(HL)(DMSO)]$^+$ (C$_{15}$H$_{17}$N$_2$O$_4$SCu$^+$).

absorbent species in equilibrium, *i.e.*, free and bound forms of **3**. Plotting the absorbance at 430 nm as a function of HSA equivalents (Fig. 6, inset) affords a sigmoidal curve that stabilizes at *ca.* [HSA]/[**3**] = 0.50, indicating that HSA can host up to two dimers or, alternatively, up to four units of the mononuclear complex derived from the dissociation of **3**. The last hypothesis is in accordance to the behaviour previously

observed for the interaction of complex **1** with HSA.[28] In fact, the spectra in Fig. 6 are identical to those obtained when studying the system HSA-**1**.

Cytotoxicity and cell proliferation studies

Cytotoxicity studies were determined by the MTT assay for complexes **1–3** on MDA-MB-231 (triple negative breast adeno-
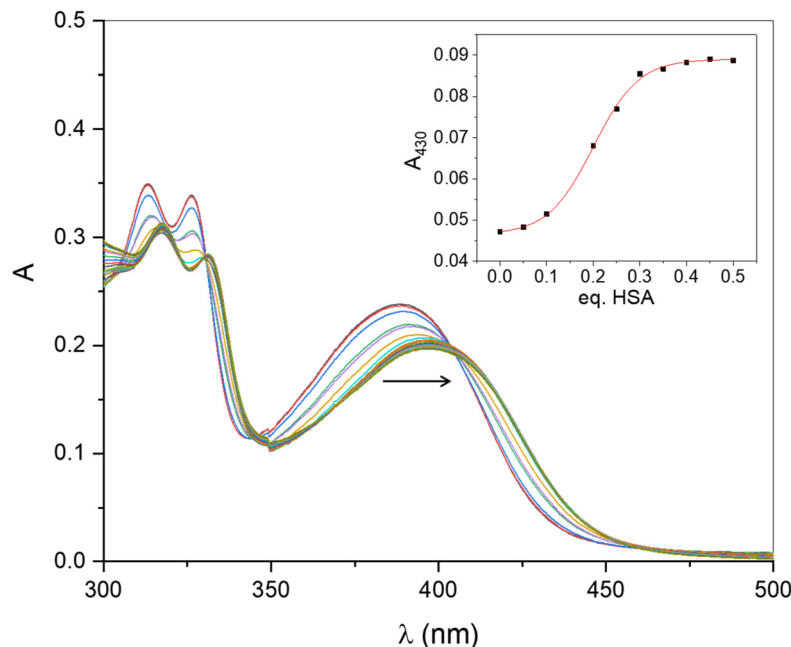
Fig. 6 UV-Vis titration of a 2×10^{-5} mol L^{-1} solution of **3** (2% MeOH/PBS, pH 7.4) with HSA at 25 °C. Inset: absorbance at 430 nm as a function of HSA equivalents; data fitted with a sigmoidal function.

carcinoma). The well-known clinical agent cisplatin (CDDP) was used as a reference for antiproliferative activity.

Table 5 shows that all the three copper compounds decreased cell viability in the submicromolar range of concentrations (0.5–2.5 μM), with similar IC$_{50}$ values for both dimers (complexes **2** and **3**, around 1.25 μM) and a slightly higher value of 2.0 μM for the monomer **1**. Given the good activity found, it seems that the charged nature of **3** does not prevent its entrance in the cell, so one can conclude that some transporter may be involved in the process. Furthermore, the fact that the antiproliferative potential of this compound is, considering standard-deviation involved, exactly double that observed for the mononuclear derivative **1** constitutes another clue supporting dissociation of **3**, previously demonstrated through EPR, electrochemical and ESI-MS, since both compounds mostly share a common derivative after their initial dissolution in DMSO (Scheme 2). Noteworthy, all the compounds are more active than CDDP, since it showed an IC$_{50}$ value of 131 μM on MDA-MB-231 cells. In addition, the IC$_{50}$ values obtained for **1–3** towards MDA-MB-231 cells are

comparable with those of the clinical drug reference doxorubicin (DOX).[31]

It must be pointed out that stability studies under conditions similar to those employed in the cell experiments (0.5% DMSO solution in PBS, pH 7.4) were performed for complexes **2** and **3**, nominally the most active ones. Upon dissolution, both compounds demonstrated to be fairly stable over a time period of 24 h (UV-Vis spectra taken over time showed only slight variations for **2** and no noticeable changes for **3**, as presented in Fig. SM1†).

On the other hand, the IC$_{50}$ values of **H$_2$L** and Cu^{2+} (free metal cation) are greater than 50 μM on the MDA-MB-231 strain, hence revealing the key role of complexation to modulate the anticancer activity of hydrazone-containing copper(II) complexes. This kind of effect has been reported for other copper complexes and other metal-based compounds.[32–34]

Previously, we have reported a series of copper(II) complexes with *N*-acylhydrazones as ligands, including [Cu(N-N-Tph)(H$_2$O)]NO$_3$ (or CuHL^1) (IC$_{50}$ = 1.6 ± 0.2 μM),[35] [Cu(N-N-BzOMe)(H$_2$O)$_2$]NO$_3$ (CuHL^2) (IC$_{50}$ = 1.6 ± 0.1 μM),[23] [Cu(N-N-BzOH)(H$_2$O)$_2$]NO$_3$ (CuHL^3) (IC$_{50}$ = 5.8 ± 0.4 μM),[18] [Cu(N-N-BzOH)(*o*-phen)] (CuHL^3/phen) (IC$_{50}$ = 5.3 ± 0.2 μM)[36] and [Cu(N-N BzOH)(bipy)]NO$_3$ (CuHL^3/bipy) (IC$_{50}$ = 11.4 ± 0.6 μM).[36] Complexes CuHL^1 and CuHL^2 displayed a similar anticancer activity in comparison with **2** and **3**. Nevertheless, CuHL^3 exhibited less activity than CuHL^1 and CuHL^2, showing the importance of methoxi above hydroxy in the benzohydrazide. Besides, the presence of coligands as *o*-phen and bipy did not improve the anticancer actions of CuHL^3. Several copper(II) complexes with vanillin derivatives and naproxen were synthetized by Lu and coworkers. Among them, the most effective

Table 5 IC$_{50}$ [μM] values of the *N*-acylhydrazonic ligand **H$_2$L** and its copper(II) complexes **1–3** on MDA-MB-231 cells after 24 h of incubation. IC$_{50}$ of complex **3** was calculated based on the dimer concentration

Compound	IC$_{50}$ [μM]
H$_2$L	>50
Cu(NO$_3$)$_2$·3H$_2$O	>50
1	2.0 ± 0.1
2	1.3 ± 0.1
3	1.2 ± 0.1
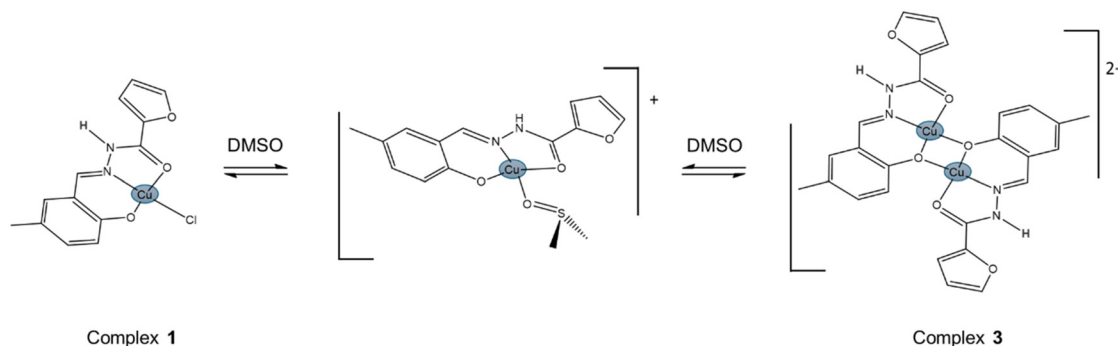
Scheme 2 Upon dissolution in a coordinating solvent as DMSO, complex **1** undergoes partial chloride substitution, while complex **3** dissociates into monomers. These processes converge in a common, positively charged mononuclear derivative, which is probably the active form of both compounds.

compound showed a moderate cytotoxicity against bulk breast cancer cells and breast cancer stem cells, with a medium micromolar cytotoxicity (37.6 ± 3.3 and 36.0 ± 4.6 μM respectively).[37]

Low and coworkers described the antitumor action of Cu^{2+} complexes containing the Schiff base N′-[1-(2-oxo-2H-chromen-3-yl)-ethylidene]-hydrazinecarbodithioic acid benzyl ester on MDA-MB-231 and MCF-7 cells, reporting IC_{50} values around 20 μM.[38]

Due to the higher activity and solution stability of complex **2**, we decided to continue the study of mechanism of action using this compound on MDA-MB-231 cells.

To evaluate the effect of **2** on the cellular reproductive potential, a clonogenic assay was performed. Fig. 7 shows a strong reduction of cell proliferation on the MDA-MB-231 strain, affecting colony formation at 0.25 μM ($p < 0.01$). Concentrations of 0.1 and 0.175 μM, instead, were unable to change basal conditions. Results agree with the cell viability assay.

ROS production

Several copper drugs can initiate pseudo-Fenton reactions intracellularly, resulting in the production of ROS.[39,40] For a good consideration of the possible mechanism involved in the cytotoxicity of complex **2** on TNBC cells, we explored the effect

of this dinuclear compound (1–15 μM) on oxidative stress using a specific probe (DHR123).[41]

The results (Table 6) evidenced that **2** increased ROS production of 242, 447 and 530% over basal levels on MDA-MB-231 cells for concentrations of 5, 10 and 15 μM after 3 h of incubation, thus suggesting that ROS production could be considered as one of the relevant mechanisms of action of compound **2**. Several reports show that many copper(II) complexes have ROS generation as an important mechanism of action related to their anticancer activity[42–44] and associated with cell death.

Table 6 ROS generation after 3 h of incubation of MDA-MB-231 cells with **2**. The results are expressed as the mean ± SEM ($n = 18$). Asterisks sign significant differences between treatments: *($p < 0.01$), **($p < 0.001$)

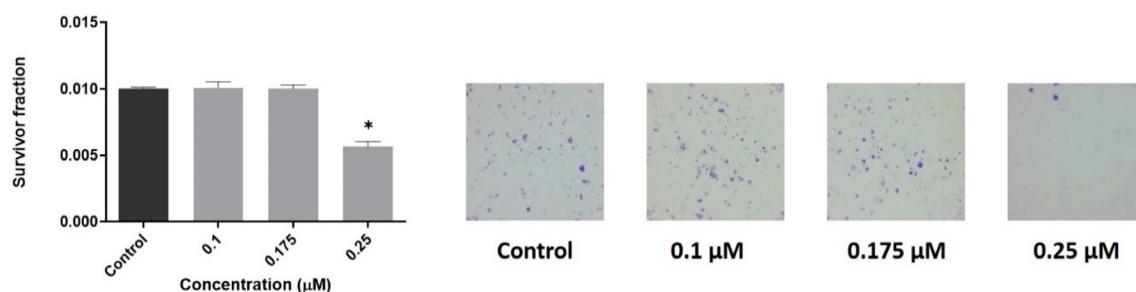| Complex 2 concentration [μM]	% ROS level
0	100.5 ± 3.2
1	97.6 ± 4.1
2.5	206.2 ± 18.6
5	242.2 ± 34.4 *
10	446.9 ± 55.8 **
15	530.4 ± 44.1 **

Fig. 7 Clonogenic assay. Effect of complex **2** on MDA–MB-231 cell viability. Cells were incubated in DMEM alone (control) or with different concentrations (0.1, 0.175 and 0.25 μM) of complex **2**. The results are expressed as surviving fraction (percentage of the basal level) and represent the mean ± the standard error of the mean (SEM) ($n = 18$). *$p < 0.01$ differences between control and treatment.

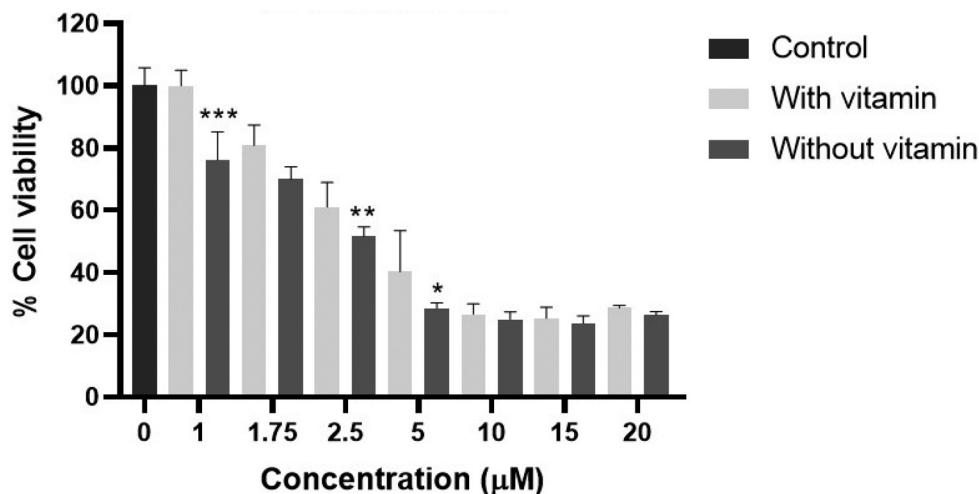**Fig. 8** Effect of complex **2** on MDA-MB-231 cell viability in the presence of a mixture of vitamins C and E (each at 50 μM). TNBC cells were incubated with different concentrations (1–20 μM) of **2** and a mixture of the vitamins at 37 °C for 3 h. The results are expressed as the mean ± SEM (n = 18). Asterisks sign significant differences between treatments: *($p < 0.01$), **($p < 0.001$), *** ($p < 0.0001$).

To confirm the importance of ROS as a mechanism of cell death by complex **2**, we carried out a cell viability assay using radical scavengers, such as a mixture of vitamins C and E, under the same experimental conditions. Fig. 8 shows that cell viability was completely recovered at [**2**] = 1 μM, whilst the deleterious effects of this complex were only partially overcome at the higher concentrations of 2.5 and 5 μM.

Apoptosis

With the aim to evaluate if **2** induces programmed cell death, we performed cell cytometry assays using annexin V (early apoptotic biomarker) and propidium iodide (PI). Fig. 9 and SM2 show the flow cytometry results of the apoptotic process in the presence of different concentrations of compound **2** (0.5, 1, 1.5 μM) on MDA-MB-231 cells. Complex **2** augmented the late apoptotic (Annexin V+/PI+) and necrotic (Annexin V−/PI+) fractions from 1 μM on. The basal condition showed 1.2% of V+/PI+ cells whilst after incubation with 1 and 1.5 μM of **2** this value increases until 31.7% and 69.6%, respectively. Also, at [**2**] = 1.5 μM, the necrotic population (V−/PI+) increased until 19.3%.

Our results are in agreement with the cell viability studies, suggesting that **2** induced cell apoptosis in a concentration-dependent manner. It is important to highlight that apoptosis
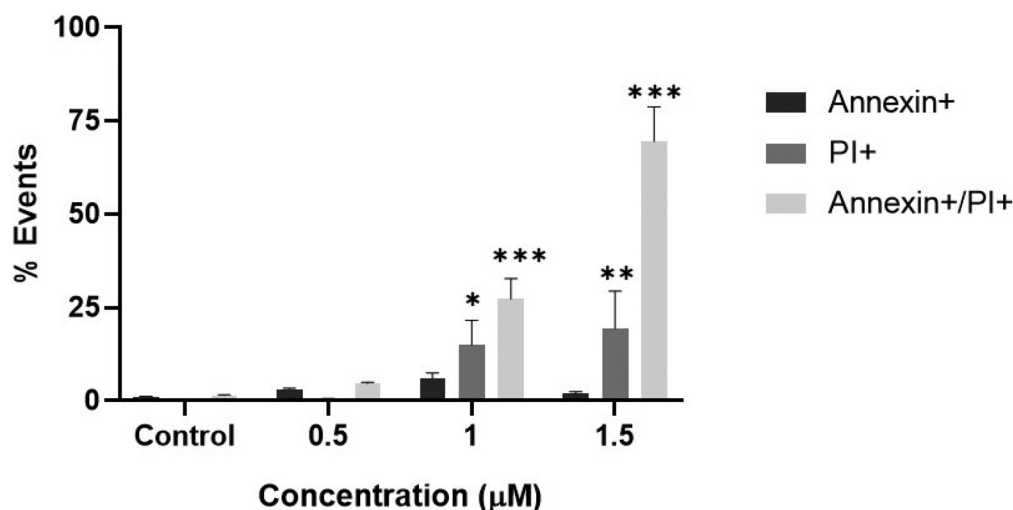

Fig. 9 Effect of complex **2** over induction of apoptosis on MDA-MB-231 cells. TNBC cells were incubated with different concentrations (0.5–1.5 μM) of **2** for 24 h. The results are expressed as the mean ± SEM (n = 9). Asterisks sign significant differences between treatments: *($p < 0.01$), **($p < 0.001$), *** ($p < 0.0001$).

Table 7 Percentage of CD44$^+$/CD24$^-$ MDA-MB-231 cells after incubation for 24 h with complex **2**. Asterisks sign significant differences between basal condition and treatment. *($p < 0.01$)

Compound [μM]	% CD44^{HIGH}/CD24^{LOW}
0	99.1
0.5	99.1
1.0	95.1 *
1.5	91.6 *

cell death have also been reported as the leading mechanism of action for many copper complexes with antitumor activity toward different cancer cell lines.[4]

Cancer stem cell studies

Solid tumors are composed of diverse cancer cell types with varying hierarchical structures.[45] In this respect, cancer stem cells (CSCs) constitute an immortal subset of the total malignant cell population with the ability to accumulate mutations that drive tumor growth.[46] CSCs play an important role in tumor aggressiveness due to their self-renewal and stemness potential. As a result, in recent years, there has been a lot of interest in developing anti-CSC medicines, and CSCs have emerged as an important and specialized cell target.[47]

In order to evaluate the anti-CSCs activity of compound **2**, we performed flow cytometry experiments using CD44 and CD24 biomarkers. Table 7 and Fig. SM3† show that **2** decreased the amount of breast CSCs on MDA-MB-231 cells. The basal condition resulted on 99.1% CD44$^+$/CD24$^-$ whilst this value is reduced after incubation with **2**, displaying 95.1% (1.0 μM) and 91.6% (1.5 μM). However, another copper(II)-hydrazone compound, CuHL$_2$, exhibited better anti-CSCs activity than complex **2** on MDA-MB-231 cells, with a reduction of CD44$^+$/CD24$^-$ population from 98.6% (basal condition) to 68.3% (at 1.5 μM).[23] Furthermore, Boodram *et al.* and Laws described the anti-CSCs activity of copper(II)-non-steroidal complexes and copper(II)-phenanthroline on breast cancer cells.[48,49]

Conclusions

The synthesis of a new dimeric complex containing the phenol-deprotonated/amide-protonated form of **H$_2$L** (5-methyl-salicylaldehyde 2-furoyl hydrazone), *i.e.* compound **3** – [Cu(**HL**)(NO$_3$)]$_2$·2H$_2$O, allowed us to establish a link between the previously published complexes **1** – [Cu(**HL**)Cl]·H$_2$O (mononuclear, phenol-deprotonated/amide-protonated) and **2** – [Cu(**L**)(i-PrOH)]$_2$ (dimeric, fully deprotonated form of the ligand). Our results indicate that the protonation status of the amide group in **H$_2$L** plays an important role in the stability of the dimer, being compound **2** (amide-deprotonated) fairly stable in solution. Conversely, complex **3**, in which the amide group remains protonated, mainly dissociates into monomers upon dissolution, as proved by UV-Vis, EPR and cyclic voltammetry. When a coordinating solvent is employed, compounds **1** and **3** generate virtually the same species: [Cu(**HL**)Solv]$^+$.

The anticancer activities of complexes **1** and **2** on MDA-MB-231 TNBC cells were assessed, and compared with that of the new analogue **3**. All the three compounds reduced cell viability in the submicromolar range of concentrations (0.5–2.5 μM), with IC$_{50}$ values around 1.25 μM for complexes **2** and **3** and a slightly higher value of 2.0 μM for the monomer **1** (which almost double the one observed for the dimers). It seems that the charged nature of the solvolysis/dissociation products of **1** and **3** does not prevent their entrance in the cell, so one can conclude that some transporter may be involved in the process. Remarkably, all the compounds are more active than the clinically used drug CDDP, by a factor of 100 in the case of **2** and **3**. Due to the high activity and solution stability of complex **2**, we decided to continue the study of mechanism of action using this compound.

Our findings highlighted that the main mechanism of action of **2** involves the ROS production and apoptosis induction. Also, this compound decreased the amount of breast CSCs, reducing the percentage of CD44$^+$/CD24$^-$ from 1.0 μM on. Taking into account the antiproliferative activity of the dimer **2** on MDA-MB-231 cells, we strongly believe that this complex is an engaging candidate for potential antitumor therapies and it would be attractive to further test it on TNBC *in vivo* experimental models.

Experimental part

Materials

Solvents and reactants were purchased from commercial sources. Human serum albumin (HSA) was bought from Sigma-Aldrich. All chemicals were used without any type of pretreatment or further purification.

Dulbecco's modified Eagle's médium (DMEM) and TrypLE™ were purchased from Gibco (Gaithersburg, MD, USA), and fetal bovine serum (FBS) was purchased from Internegocios (Argentina). Tissue culture materials were purchased from Corning (Princeton, NJ, USA). Annexin V, fluorescein isothiocyanate (FITC), propidium iodide (PI), DHR123 and Dihydroetidium were from Invitrogen (Buenos Aires, Argentina). CD44 and CD24 antibodies were purchased by BD (USA).

Methods

Syntheses. H$_2$L was prepared as previously described.[28] M.p. = 150 ± 2 °C. ^{1}H NMR (DMSO-d_6, ppm): 12.08 (s, 1H, –N*H*–); 10.88 (s, 1H, –O*H*); 8.60 (s, 1H, *H*7); 7.96 (dd, 1H, *H*12); 7.34 (bs, 1H, *H*5); 7.31 (d, 1H, *H*10); 7.10 (dd, 1H, *H*3); 6.82 (d, 1H, *H*2); 6.71 (dd, 1H, *H*11); 2.25 (s, 3H, *H*13). TGA: a two-step weight loss of approximately 6.7% (calcd 6.9%) is observed between 60 and 160 °C, consistent with a hydration water molecule. Mid IR (KBr, cm^{-1}): 3225 [ν(N–H)$_{hydrazone}$]; 3202 [ν(O–H)$_{phenol}$]; 1653 [ν(C=O)]; 1628 [ν(C=N)$_{hydrazone}$]; 1495 [δ(C–N–H)$_{hydrazone}$]; 1326 [ν(C–O)$_{phenol}$]; 1164 [ν(N–N)].

[Cu(C$_{13}$H$_{11}$O$_3$N$_2$)(NO$_3$)]$_2$·2H$_2$O (**3**). 242 mg of Cu(NO$_3$)$_2$·3H$_2$O (1.0 mmol) were dissolved in 10 mL MeOH and

dropwise added to 15 mL of a **H₂L** methanolic solution (262 mg, 1.0 mmol). The reactants were stirred at room temperature for 1 h, affording a dark green solution. After a few days on the bench, green crystals suitable for XRD analysis were isolated. Yield = 310 mg (0.40 mmol of dimer, 80%). Elemental analysis (%) – calculated for [Cu(C₁₃H₁₁O₃N₂)(NO₃)]₂·2H₂O (773.60 g mol⁻¹): C – 40.4, H – 3.4, N – 10.9; found: C – 39.9, H – 3.0, N – 10.6. ICP-OES (%) – calculated: Cu – 16.4; found: Cu – 16.2. TGA: a weight loss of approximately 4.6% (calcd 4.6%) between 110 and 145 °C, consistent with the removal of two hydration water molecules per dimer. Mid IR (KBr, cm⁻¹): 3198 [ν(N–H)$_{hydrazone}$]; 1630 [ν(C=O)]; 1610 [ν(C=N)$_{hydrazone}$]; 1610 [ν(C=N)$_{hydrazone}$]; 1384 [ν(NO₂)$_{as\ nitrate}$]; 1345 [ν(C–O)$_{phenol}$]; 1305 [ν(NO₂)$_{sym\ nitrate}$]; 1118 [ν(N–N)].

Molar conductivity in DMF: 160.4 ohm⁻¹ cm² mol⁻¹ (equivalent to a 1 : 2 electrolyte system),[50] indicating that both nitrate ions are dissociated upon dissolution. In DMSO, the value of 112 ohm⁻¹ cm² mol⁻¹ was obtained, also in agreement with a 1 : 2-type electrolyte (expected range: 110–195 ohm⁻¹ cm² mol⁻¹, according to the reference by Ali *et al.*)[51]

Physicochemical analyses

Crystal data. Single-crystal XRD data for **3** were collected in a Rigaku Synergy diffractometer using CuKα (λ = 1.54184 Å) radiation at room temperature (298 K). Data collection and reduction, as well as cell refinement, were performed using the CRYSALISPRO software.[52] The structures were resolved and refined by SHELX[53] using OLEX2 system,[54] and all non-hydrogen atoms were refined with anisotropic thermal parameters. H atoms connected to carbon were placed in idealized positions and treated by a rigid model, with Uiso(H) = 1.2 Ueq for aromatic rings and CH groups. The figures were drawn using ORTEP-3 for Windows[55] and Mercury[56] programs.

Spectroscopy. Mid-infrared (Mid IR) vibrational spectra were acquired on a PerkinElmer Spectrum 100 FTIR spectrophotometer, at room temperature, in KBr pellets, in the 4000–400 cm⁻¹ range with resolution of 4 cm⁻¹. UV-Vis absorption (electronic) spectra, over the wavelength range 250–800 nm, were recorded in an Agilent spectrophotometer Cary 100 Conc, after dissolving the compounds in DMF. In the case of the complexation study of the ligand, the measurements were performed using methanolic solutions in order to emulate the synthetic conditions employed in the preparation of compound **3**, using [**H₂L**] = 2 × 10⁻⁵ mol L⁻¹ and adding successive 0.05 eq. increments of a copper(II) nitrate trihydrate solution. The ligand **H₂L** was characterized by ¹H NMR spectroscopy as well. The spectrum was recorded on a Bruker Avance III HD-400 spectrometer, calibrated in reference to the residual peak for DMSO-d_6 (2.50 ppm) and processed with the TopSpin 3.6.5 software. EPR spectra of **3** were recorded at 300 K (room temperature, solid state) or 77 K (liquid nitrogen, DMF and DMSO solutions) on a CW-Bruker EMX-Plus spectrometer with X-band cavity (9.5 GHz), employing microwave powers of 10 mW, with a 100 kHz modulation field of about 1 Oe in amplitude. Spectra were fitted using theEasyspin[45] MATLAB routine.

CHNS and copper content. Elemental analyses were performed in a CHN 2400 PerkinElmer instrument. All the measurements were carried out in duplicate. On the other hand, copper content in complex **3** was estimated using an inductively coupled plasma optical emission ICP-OES PerkinElmer Optima 7300 DV spectrometer. Sample was treated with nitric acid and diluted in water. Measurements were done with the dye laser pulsed in the 324.7 nm line.

Thermogravimetric analysis and electrical conductivity. The thermogravimetric curve of **3** was acquired in a Thermogravimetric Analyzer PerkinElmer, Pyris 1 TGA. TGA scans were performed from 25 to 900 °C at 10 °C min⁻¹ under nitrogen flow. Curve optimization and calculations were processed in the Pyris v 8.0.0.0172 software. Conductivity measurements were performed at room temperature in a Metrohm 856 electrical conductivimeter equipped with a 900 Touch Control. Complex **3** was dissolved in DMF or DMSO at a final concentration of 1 × 10⁻³ mol L⁻¹.

Cyclic voltammetry. Cyclic voltammetry was performed at room temperature in a BASi Epsilon™ EC potenciostat/galvanostat. Experiments were carried out in DMF solution with 0.1 mol L⁻¹ Bu₄NPF₆ as supporting electrolyte, under nitrogen atmosphere, in a three-electrode cell. A 3.0 mm diameter Glassy Carbon Electrode was employed as the working electrode. Reference was the BASi MF-2052 Ag/AgCl (3 mol L⁻¹ NaCl) electrode, while the counter-electrode consisted of a platinum wire.

Electrospray ionization mass spectrometry. ESI-MS data were collected on a Bruker Daltonics impact HD mass spectrometer, in the positive mode. A stock solution of the sample was prepared by dissolving 2.0 mg of **3** in 1.0 mL of DMSO. A 10 μL aliquot of this solution was diluted in 1990 μL of methanol (200×) and analysed by direct infusion. Standard configuration parameters were used.

Solution stability of the complexes. Stock solutions of compounds **2** and **3** were prepared in DMSO and then diluted with PBS (pH 7.4) to a concentration of 2 × 10⁻⁵ mol L⁻¹, final DMSO content of 0.5%. These solutions were monitored over 24 h by UV-Vis spectrophotometry in the range 250–500 nm.

HSA-binding studies. The experimental interaction between HSA and the dinuclear coordination compound **3** was confirmed by UV-Vis spectroscopy (Cary 100 Conc). Solution of the complex was prepared at 2 × 10⁻⁵ mol L⁻¹. **3** was dissolved in 2% MeOH/PBS (50 × 10⁻³ mol L⁻¹, pH 7.4). On the other hand, HSA stock solution (3 × 10⁻⁴ mol L⁻¹) was prepared in pure PBS. 3,0 mL of complex solution were placed in the cuvette and equal amounts (10 μL) of HSA were added at each titration point. All measurements were carried out at 25 °C.

Cell line and growth conditions. MDA-MB-231 (ATCC HTB-26) were grown in DMEM-F12 (Dulbecco's modified Eagle's medium F12) containing 10% fetal bovine serum (FBS), 100 IU mL⁻¹ penicillin and 100 μg mL⁻¹ streptomycin at 37 °C in 5% CO₂ atmosphere.

Cell viability study with and without scavengers. For the cytotoxicity studies, we firstly dissolved the compounds in pure DMSO at a concentration of 5 mM, and then dilute to 25 μM with DMEM-F12 (final DMSO amount in the stock solution: 0.5%). The MTT assay was performed according to Mosmann *et al.*[57] Briefly, cells were seeded in a 96-multiwell dish, allowed to attach for 24 h and treated with different concentrations of complexes **1–3**, **H₂L** and Cu(NO₃)₂·3H₂O at 37 °C for 24 h. Afterward, medium was changed and cells were incubated with 0.5 mg mL⁻¹ MTT under normal culture conditions for 3 h. Cell viability was marked by the conversion of the tetrazolium salt MTT [3-(4,5-dimethylthiazol-2-yl)-2,5-diphenyltetrazolium bromide] to a coloured formazan by mitochondrial dehydrogenases. Colour development was measured spectrophotometrically in a microplate reader (model 7530, Cambridge technology, Inc., USA) at 570 nm after cell lysis in DMSO (100 μL per well). Cell viability was plotted as the percentage of the control value. To evaluate the potential recovery of cell viability for the use of scavengers, we carried out the cell viability assays in the same condition but with the presence of a mixture of vitamins C and E (each at 50 μM).

Clonogenic assay. Cells were seeded in 24 well plates, after attachment of the cells to the dishes, they were treated with complex **2** at a range of 0.1 to 0.25 μM. After 24 h, the cells were washed with PBS and 2 mL of complete DMEM were added. Plates were incubated for 10 days at 37 °C and 5% CO₂. After this time, medium was removed, and cells were rinsed with PBS. Cells were stained with a mixture of 6% of glutaraldehyde and 0.5% of crystal violet for 30 minutes at room temperature. Then, the plates were washed with distilled water and dried. After that, we proceed to count the colonies. The plating efficiency (PE) is the ratio of the number of colonies to the number of cells seeded whilst the number of colonies that survive after treatment, expressed in terms of PE, is called the surviving fraction (SF).

Reactive oxygen species studies. Oxidative stress was evaluated in the MDA-MB-231 cell line by measurement of intracellular production of ROS after incubation of the cell monolayers with different concentrations of complex **2** for 24 h at 37 °C. ROS generation was determined by oxidation of Dihydrorhodamine 123 to rodamine by spectrofluorimetry.

Apoptosis. Cells in early and late stages of apoptosis were detected through Annexin V-FITC (fluorescein isothiocyanate) and PI (propidium iodide) staining. Cells were treated with the compound **2** for 24 h prior to analysis. For the staining, the cells were washed with PBS and then diluted with 1 μL binding buffer. To 100 μL of cell suspension, 2.5 μL of Annexin V-FITC and 2 μL PI (250 mg mL⁻¹) were added and incubated for 15 min at room temperature. Cells were analysed using a BD Accuri C6 Plus flow cytometer with the BD Accuri C6 Plus software. For each analysis 10 000 counts, gated on an FSC *vs.* SSC dot plot, were recorded.

Cancer stem cell studies. MDA-MB-231 cells were collected and monoclonal antibodies against human CD44-FITC and CD24PE (BD Biosciences, USA) were added to cell suspension in recommended concentration and incubated at room temperature in dark for 30 min. Then, cells were washed with phosphate-buffered saline (PBS) and analysed by the BD Accuri C6 Plus.

Statistical analysis. Results are expressed as the mean of three independent experiments and plotted as mean ± standard error of the mean (SEM). The total number of repeats (n) is specified in the legends of the figures. Statistical differences were analysed using the analysis of variance method followed by the test of least significant difference (Fisher). The statistical analyses were performed using STATGRAPHICS Centurion XVI.I.

Data availability

The data supporting this article have been included as part of the ESI (Fig. SM1 and Fig. SM2†).

Crystallographic data for complex **3** has been deposited with the Cambridge Crystallographic Data Centre as Suppl. Publications CCDC 2370060.†

Conflicts of interest

There are no conflicts to declare.

Acknowledgements

References

1 I. O. Alanazi and Z. Khan, Understanding EGFR Signaling in Breast Cancer and Breast Cancer Stem Cells: Overexpression and Therapeutic Implications, *Asian Pac. J. Cancer Prev.*, 2016, **17**(2), 445–453, DOI: **10.7314/APJCP.2016.17.2.445**.

2 S. Wen, L. Manuel, M. Doolan, J. Westhuyzen, T. P. Shakespeare and N. J. Aherne, Effect of Clinical and Treatment Factors on Survival Outcomes of Triple Negative Breast Cancer Patients, *Breast Cancer: Targets Ther.*, 2020, **12**, 27–35, DOI: **10.2147/BCTT.S236483**.

3 R. Nanda, Novel therapies for triple-negative breast cancer, *Clin. Adv. Hematol. Oncol.*, 2020, **18**(12), 799–801.

4 L. M. Balsa, E. J. Baran and I. E. León, Copper Complexes as Antitumor Agents: In vitro and In vivo Evidence, *Curr. Med. Chem.*, 2023, **30**(5), 510–557, DOI: **10.2174/0929867328666211117094550**.

5 V. Ferretti and I. León, An Overview of Vanadium and Cell Signaling in Potential Cancer Treatments, *Inorganics*, 2022, **10**(4), 47, DOI: **10.3390/inorganics10040047**.

6 E. J. Anthony, E. M. Bolitho, H. E. Bridgewater, *et al.*, Metallodrugs are unique: opportunities and challenges of discovery and development, *Chem. Sci.*, 2020, **11**(48), 12888–12917, DOI: **10.1039/D0SC04082G**.

7 I. Ott and R. Gust, Non Platinum Metal Complexes as Anti–cancer Drugs, *Arch. Pharm.*, 2007, **340**(3), 117–126, DOI: **10.1002/ardp.200600151**.

8 I. Leon, J. Cadavid-Vargas, A. Di Virgilio and S. Etcheverry, Vanadium, Ruthenium and Copper Compounds: A New Class of Nonplatinum Metallodrugs with Anticancer Activity, *Curr. Med. Chem.*, 2017, **24**(2), 112–148, DOI: **10.2174/0929867323666160824162546**.

9 D. Denoyer, S. A. Clatworthy and M. A. Cater, *Metallo-Drugs: Development and Action of Anticancer Agents*, ed. A. Sigel, H. Sigel, E. Freisinger and R.KO. Sigel, De Gruyter, 2018, vol. 18. DOI: **10.1515/9783110470734**.

10 V. Gandin, C. Ceresa, G. Esposito, *et al.*, Therapeutic potential of the phosphino Cu(I) complex (HydroCuP) in the treatment of solid tumors, *Sci. Rep.*, 2017, **7**(1), 13936, DOI: **10.1038/s41598-017-13698-1**.

11 C. Santini, M. Pellei, V. Gandin, M. Porchia, F. Tisato and C. Marzano, Advances in Copper Complexes as Anticancer Agents, *Chem. Rev.*, 2014, **114**(1), 815–862, DOI: **10.1021/cr400135x**.

12 R. Alemón-Medina, M. Breña-Valle, J. L. Muñoz-Sánchez, M. I. Gracia-Mora and L. Ruiz-Azuara, Induction of oxidative damage by copper-based antineoplastic drugs (Casiopeínas®), *Cancer Chemother. Pharmacol.*, 2007, **60**(2), 219–228, DOI: **10.1007/s00280-006-0364-9**.

13 J. F. Cadavid-Vargas, I. E. Leon, S. B. Etcheverry, E. Santi, M. H. Torre and A. L. Di Virgilio, Copper(II) Complexes with Saccharinate and Glutamine as Antitumor Agents: Cytoand Genotoxicity in Human Osteosarcoma Cells, *Anticancer Agents Med. Chem.*, 2017, **17**(3), 424–433, DOI: **10.2174/1871520616666160513130204**.

14 L. M. Balsa, M. C. Ruiz, L. Santa Maria de la Parra, E. J. Baran and I. E. León, Anticancer and antimetastatic activity of copper(II)-tropolone complex against human breast cancer cells, breast multicellular spheroids and mammospheres, *J. Inorg. Biochem.*, 2020, **204**, 110975, DOI: **10.1016/j.jinorgbio.2019.110975**.

15 L. M. Balsa, V. Ferretti, M. Sottile, *et al.*, New copper(II) and oxidovanadium(IV) complexes with a vitamin B6 Schiff base: mechanism of action and synergy studies on 2D and 3D human osteosarcoma cell models, *Dalton Trans.*, 2024, **53**(7), 3039–3051, DOI: **10.1039/D3DT02964F**.

16 X. Shi, Z. Chen, Y. Wang, Z. Guo and X. Wang, Hypotoxic copper complexes with potent anti-metastatic and anti-angiogenic activities against cancer cells, *Dalton Trans.*, 2018, **47**(14), 5049–5054, DOI: **10.1039/C8DT00794B**.

17 M. R. Rodríguez, L. M. Balsa, J. Del Plá, *et al.*, Synthesis, characterization, DFT calculations and anticancer activity of a new oxidovanadium(IV) complex with a ligand derived from o-vanillin and thiophene, *New J. Chem.*, 2019, **43**(29), 11784–11794, DOI: **10.1039/C9NJ02092F**.

18 Y. Burgos-Lopez, J. Del Plá, L. M. Balsa, *et al.*, Synthesis, crystal structure and cytotoxicity assays of a copper(II) nitrate complex with a tridentate ONO acylhydrazone ligand. Spectroscopic and theoretical studies of the complex and its ligand, *Inorg. Chim. Acta*, 2019, **487**, 31–40, DOI: **10.1016/j.ica.2018.11.039**.

19 S. D. Joshi, D. Kumar, S. R. Dixit, *et al.*, Synthesis, characterization and antitubercular activities of novel pyrrolyl hydrazones and their Cu-complexes, *Eur. J. Med. Chem.*, 2016, **121**, 21–39, DOI: **10.1016/j.ejmech.2016.05.025**.

20 A. K. Tanoli, Z. Khan, T. Kamal, M. Ali, M. Latif and Z. T. Maqsood, Metal-based biologically active compounds: Synthesis, spectral and antioxidant studies of transition metal complexes with hydrazone derivatives, *Pak. J. Pharm. Sci.*, 2019, **32**(1), 103–108.

21 S. Thota and D. A. Rodrigues, Pinheiro P de SM, Lima LM, Fraga CAM, Barreiro EJ, N-Acylhydrazones as drugs, *Bioorg. Med. Chem. Lett.*, 2018, **28**(17), 2797–2806, DOI: **10.1016/j.bmcl.2018.07.015**.

22 L. Santa Maria de la Parra, A. I. B. Romo, J. Rodríguez-López, *et al.*, Promising Dual Anticancer and Antimetastatic Action by a Cu(II) Complex Derived from Acylhydrazone on Human Osteosarcoma Models, *Inorg. Chem.*, 2024, **63**(11), 4925–4938, DOI: **10.1021/acs.inorgchem.3c04085**.

23 L. M. Balsa, V. Ferraresi-Curotto, M. J. Lavecchia, *et al.*, Anticancer activity of a new copper(II) complex with a hydrazone ligand. Structural and spectroscopic characterization, computational simulations and cell mechanistic studies on 2D and 3D breast cancer cell models, *Dalton Trans.*, 2021, **50**(28), 9812–9826, DOI: **10.1039/D1DT00869B**.

24 M. R. Rodríguez, L. M. Balsa, O. E. Piro, *et al.*, Synthesis, Crystal Structure, Spectroscopic Characterization, DFT Calculations and Cytotoxicity Assays of a New Cu(II) Complex with an Acylhydrazone Ligand Derived from Thiophene, *Inorganics*, 2021, **9**(2), 9, DOI: **10.3390/inorganics9020009**.

25 JP Rada, J Forté, G Gontard, *et al.*, Novel luminescent benzopyranothiophene- and BODIPY-derived aroylhydrazonic ligands and their dicopper(II) complexes: syntheses, antiproliferative activity and cellular uptake studies, *Anticancer Agents Med. Chem.*, 2021, **26**(6), 675–688, DOI: **10.1007/s00775-021-01885-5**.

26 J. P. Rada, J. Forté, G. Gontard, V. Corcé, M. Salmain and N. A. Rey, Isoxazole–Derived Aroylhydrazones and Their Dinuclear Copper(II) Complexes Show Antiproliferative Activity on Breast Cancer Cells with a Potentially Alternative Mechanism Of Action, *ChemBioChem*, 2020, **21**(17), 2474–2486, DOI: **10.1002/cbic.202000122**.

27 J. P. Rada, B. S. M. Bastos, L. Anselmino, *et al.*, Binucleating Hydrazonic Ligands and Their μ-Hydroxodicopper(II) Complexes as Promising Structural Motifs for Enhanced Antitumor Activity, *Inorg. Chem.*,

2019, **58**(13), 8800–8819, DOI: **10.1021/acs.inorgchem.9b01195**.

28 F. d. S. Moura, Y. S. Sobrinho, C. Stellet, *et al.*, Copper(ɪɪ) complexes of a furan-containing aroylhydrazonic ligand: syntheses, structural studies, solution chemistry and interaction with HSA, *Dalton Trans.*, 2023, **52**(47), 17731–17746, DOI: **10.1039/D3DT02597G**.

29 U. Sakaguchi and A. W. Addison, Spectroscopic and redox studies of some copper(ɪɪ) complexes with biomimetic donor atoms: implications for protein copper centres, *J. Chem. Soc., Dalton Trans.*, 1979, (4), 600, DOI: **10.1039/dt9790000600**.

30 D. Kivelson and R. Neiman, ESR Studies on the Bonding in Copper Complexes, *J. Chem. Phys.*, 1961, **35**(1), 149–155, DOI: **10.1063/1.1731880**.

31 N. Ayoub, K. Al-Shami, M. A. Y. Alqudah and N. Mhaidat, Crizotinib, a MET inhibitor, inhibits growth, migration, and invasion of breast cancer cells in vitro and synergizes with chemotherapeutic agents, *OncoTargets Ther.*, 2017, **10**, 4869–4883, DOI: **10.2147/OTT.S148604**.

32 MR Rodríguez, J Del Plá, LM Balsa, *et al.*, Cu(ɪɪ) and Zn(ɪɪ) complexes with a poly-functional ligand derived from o-vanillin and thiophene. Crystal structure, physico-chemical properties, theoretical studies and cytotoxicity assays against human breast cancer cells, *New J. Chem.*, 2019, **43**(18), 7120–7129, DOI: **10.1039/C8NJ06274A**.

33 A. I. Matesanz, E. Jimenez-Faraco, M. C. Ruiz, *et al.*, Mononuclear Pd(ɪɪ) and Pt(ɪɪ) complexes with an α-N-heterocyclic thiosemicarbazone: cytotoxicity, solution behaviour and interaction versus proven models from biological media, *Inorg. Chem. Front.*, 2018, **5**(1), 73–83, DOI: **10.1039/C7QI00446J**.

34 A. C. González-Baró, V. Ferraresi-Curotto, R. Pis-Diez, *et al.*, A novel oxidovanadium(v) compound with an isonicotino-hydrazide ligand. A combined experimental and theoretical study and cytotoxity against K562 cells, *Polyhedron*, 2017, **135**, 303–310, DOI: **10.1016/j.poly.2017.07.013**.

35 L. M. Balsa, M. R. Rodriguez, B. S. Parajón-Costa, A. C. González-Baró, M. J. Lavecchia and I. E. León, Anticancer Activity and Mechanism of Action Evaluation of an Acylhydrazone Cu(ɪɪ) Complex toward Breast Cancer Cells, Spheroids, and Mammospheres, *ChemMedChem*, 2022, **17**(4), DOI: **10.1002/cmdc.202100520**.

36 Y. Burgos-López, L. M. Balsa, O. E. Piro, *et al.*, Tridentate acylhydrazone copper(ɪɪ) complexes with heterocyclic bases as coligands. Synthesis, spectroscopic studies, crystal structure and cytotoxicity assays, *Polyhedron*, 2022, **213**, 115621, DOI: **10.1016/j.poly.2021.115621**.

37 C. Lu, A. Eskandari, P. B. Cressey and K. Suntharalingam, Cancer Stem Cell and Bulk Cancer Cell Active Copper(ɪɪ) Complexes with Vanillin Schiff Base Derivatives and Naproxen, *Chem. – Eur. J.*, 2017, **23**(47), 11366–11374, DOI: **10.1002/chem.201701939**.

38 M. L. Low, G. Paulus, P. Dorlet, *et al.*, Synthesis, characterization and biological activity of Cu(ɪɪ), Zn(ɪɪ) and Re(ɪ) complexes derived from S-benzyldithiocarbazate and 3-acetyl-

coumarin, *BioMetals*, 2015, **28**(3), 553–566, DOI: **10.1007/s10534-015-9831-2**.

39 U. Jungwirth, C. R. Kowol, B. K. Keppler, C. G. Hartinger, W. Berger and P. Heffeter, Anticancer Activity of Metal Complexes: Involvement of Redox Processes, *Antioxid. Redox Signaling*, 2011, **15**(4), 1085–1127, DOI: **10.1089/ars.2010.3663**.

40 I. Garcia-Bosch and M. A. Siegler, Copper-Catalyzed Oxidation of Alkanes with H_2O_2 under a Fenton-like Regime, *Angew. Chem., Int. Ed.*, 2016, **55**(41), 12873–12876, DOI: **10.1002/anie.201607216**.

41 M. Yazdani, Concerns in the application of fluorescent probes DCDHF-DA, DHR 123 and DHE to measure reactive oxygen species in vitro, *Toxicol. In Vitro*, 2015, **30**(1 Pt B), 578–582, DOI: **10.1016/j.tiv.2015.08.010**.

42 A. I. B. Romo, V. S. Dibo, D. S. Abreu, *et al.*, Ascorbyl and hydroxyl radical generation mediated by a copper complex adsorbed on gold, *Dalton Trans.*, 2019, **48**(37), 14128–14137, DOI: **10.1039/C9DT01726G**.

43 M. C. Ruiz, K. Perelmulter, P. Levín, *et al.*, Antiproliferative activity of two copper(ɪɪ) complexes on colorectal cancer cell models: Impact on ROS production, apoptosis induction and NF-κB inhibition, *Eur. J. Pharm. Sci.*, 2022, **169**, 106092, DOI: **10.1016/j.ejps.2021.106092**.

44 P. Levín, M. C. Ruiz, A. I. B. Romo, *et al.*, Water-mediated reduction of [Cu(dmp)2(CH₃CN)]2+: implications of the structure of a classical complex on its activity as an anticancer drug, *Inorg. Chem. Front.*, 2021, **8**(13), 3238–3252, DOI: **10.1039/D1QI00233C**.

45 M. C. Cabrera, R. E. Hollingsworth and E. M. Hurt, Cancer stem cell plasticity and tumor hierarchy, *World J. Stem Cells*, 2015, **7**(1), 27–36, DOI: **10.4252/wjsc.v7.i1.27**.

46 M. Z. Ratajczak, Cancer stem cells–normal stem cells "Jedi" that went over to the "dark side", *Folia Histochem. Cytobiol.*, 2005, **43**(4), 175–181.

47 M. De Angelis, F. Francescangeli and A. Zeuner, Breast Cancer Stem Cells as Drivers of Tumor Chemoresistance, Dormancy and Relapse: New Challenges and Therapeutic Opportunities, *Cancers*, 2019, **11**(10), 1569, DOI: **10.3390/cancers11101569**.

48 K. Laws, G. Bineva-Todd, A. Eskandari, C. Lu, N. O'Reilly and K. Suntharalingam, A Copper(ɪɪ) Phenanthroline Metallopeptide That Targets and Disrupts Mitochondrial Function in Breast Cancer Stem Cells, *Angew. Chem., Int. Ed.*, 2018, **57**(1), 287–291, DOI: **10.1002/anie.201710910**.

49 J. N. Boodram, I. J. Mcgregor, P. M. Bruno, P. B. Cressey, M. T. Hemann and K. Suntharalingam, Breast Cancer Stem Cell Potent Copper(ɪɪ)–Non-Steroidal Anti-Inflammatory Drug Complexes, *Angew. Chem., Int. Ed.*, 2016, **55**(8), 2845–2850, DOI: **10.1002/anie.201510443**.

50 W. J. Geary, The use of conductivity measurements in organic solvents for the characterisation of coordination compounds, *Coord. Chem. Rev.*, 1971, **7**(1), 81–122, DOI: **10.1016/S0010-8545(00)80009-0**.

51 I. Ali, W. A. Wani and K. Saleem, Empirical Formulae to Molecular Structures of Metal Complexes by Molar

Conductance, *Synth. React. Inorg., Met.-Org., Nano-Met. Chem.*, 2013, **43**(9), 1162–1170, DOI: **10.1080/15533174.2012.756898**.

52 Rigaku Oxford Diffraction, *CrysAlisPRO, version 11713846*, Rigaku Corporation, Tokyo, Japan. Published online 2015.

53 G. M. Sheldrick, Crystal structure refinement with SHELXL, *Acta Crystallogr., Sect. C: Struct. Chem.*, 2015, **71**(1), 3–8, DOI: **10.1107/S2053229614024218**.

54 O. V. Dolomanov, L. J. Bourhis, R. J. Gildea, J. A. K. Howard and H. Puschmann, OLEX2: a complete structure solution, refinement and analysis program, *J. Appl. Crystallogr.*, 2009, **42**(2), 339–341, DOI: **10.1107/S0021889808042726**.

55 L. J. Farrugia, WinGX and ORTEP for Windows: an update, *J. Appl. Crystallogr.*, 2012, **45**(4), 849–854, DOI: **10.1107/S0021889812029111**.

56 C. F. Macrae, I. J. Bruno, J. A. Chisholm, *et al.*, Mercury CSD 2.0 – new features for the visualization and investigation of crystal structures, *J. Appl. Crystallogr.*, 2008, **41**(2), 466–470, DOI: **10.1107/S0021889807067908**.

57 T. Mosmann, Rapid colorimetric assay for cellular growth and survival: Application to proliferation and cytotoxicity assays, *J. Immunol. Methods*, 1983, **65**(1–2), 55–63, DOI: **10.1016/0022-1759(83)90303-4**.